P9.8 THE SOUTHWEST OHIO MINISUPERCELL TORNADO OUTBREAK OF 11 JULY 2006. PART II: INVESTIGATION INTO REAR-FLANK DOWNDRAFT FORMATION AND ITS RELATION TO TORNADOGENESIS

Daniel P. Hawblitzel*
NOAA/National Weather Service, Wilmington, OH

1. INTRODUCTION

Rear-flank downdrafts (RFDs) have a well-established association with near-ground vertical vorticity in supercells, an ingredient that is needed for tornadogenesis. However, how the RFD acquires vertical vorticity is not well understood. In addition, the dominant forcing mechanisms for RFDs remain unknown, with many existing proposals among researchers. Prior literature has indicated that midlevel, dynamically-induced positive pressure perturbations may force an RFD downward (see Markowski 2002). Positive pressure perturbations may be caused by convergence and divergence or deformation, and may be located upshear of an updraft. Additionally, the modeling study of Klemp and Rotunno (1983) proposed that dynamic negative pressure perturbations associated with a strong low-level circulation can induce a downward-directed pressure gradient which intensifies the RFD during the occlusion phase of the low-level mesocyclone, a phenomenon known as the occlusion downdraft.

While most numerical simulations and high-resolution radar analyses of supercell storms have concentrated on Great Plains environments with moderate-to-high values of CAPE and shear, some studies have documented important characteristics of supercells in low-CAPE, high low-level shear environments, such as a landfalling tropical cyclone. McCaul and Weisman (1996) found that when both buoyancy and shear were maximized near 3-4 km, their simulated storms resembled the dynamic pressure-driven lower portions of Great Plains supercells, lacking only their highly buoyant upper-tropospheric parts. They demonstrated that these pressure-driven updrafts may rival their Great Plains counterparts in intensity in the low levels, but because of limited buoyancy, this forcing quickly destroys updraft strength at higher altitudes. Their simulation using an observed Centreville, Alabama sounding during 1985's Hurricane Danny (referred to as the CKL simulation in their study) indicated a quick deceleration of the updraft around 2-3 km. In an observational study, Schneider and Sharp (2007) composited radar characteristics of several hurricane-spawned tornadic supercells over North Carolina during the active 2004 hurricane season. They noted a particularly interesting signature which preceded 14 of the 15 tornado events in that study. This feature, which they termed a velocity enhancement signature (VES), appeared as a small area of enhanced radial velocity of 30 kt or greater, usually between 2 and 4 km AGL. They found that in all its occurrences, the VES was located above the low-level inflow region of the storm, and was collocated with the hook and low-level rotation, when present. They speculated that the VES may be related to the formation of the RFD due to its location relative to the mesocyclone.

The purpose of this paper is to examine WSR-88D observations of a tornadic minisupercell during a localized tornado outbreak over southwest Ohio on 11 July 2006. It was revealed in Hawblitzel (2008) that the environment over southwest Ohio that evening was comparable to a tropical cyclone tornado setting which favored minisupercells (with an environmental sounding quite similar to the CKL case in McCaul and Weisman 1996). This study takes advantage of the relatively rare event in which a tornadic minisupercell passes very near a WSR-88D radar, in which case detailed reflectivity and velocity signatures can be detected throughout a significant depth of the storm.

2. METHODOLOGY

This study presents an analysis of KILN WSR-88D radar data from 11 July 2006. The Weather Event Simulator and Four-Dimensional Stormcell Investigator are used to examine the radar data. The primary storm to be analyzed is a minisupercell which tracked within 8 km of the KILN radar and allowed for radar data with azimuthal resolution as high as 150 m and base data as low as 120 m AGL. Range resolution is 250 m for velocity data and 1 km for reflectivity. Even though the cone of silence usually places significant limitations on mid-and upper-level storm data this close to the radar, this constraint was not as much of a concern in this case due to the shallow nature of the storm.

3. RADAR ANALYSIS

Figure 1 shows four elevation slices of the minisupercell of interest as it underwent a quick intensification of the updraft and mesocyclone at 0006 UTC on 12 July. At this time, the mesocyclone was characterized by relatively strong easterly inflow below cloud base (Fig. 1a), transitioning to a balanced circulation inside the weak echo region around 1.4 km AGL (Fig. 1c), then being dominated by westerly storm-relative flow along its southern flank in its upper portions (Fig. 1e). Above the mesocyclone, an area of enhanced westerly velocity is evident, flowing away from the center of the mesocyclone (Fig. 1g). This feature appears very similar to the VES introduced by Schneider and Sharp (2007), so the same terminology will be used to annotate the velocity signature here. This vertical flow pattern suggests a gyre circulation,

* *Corresponding author address: Daniel P. Hawblitzel, NOAA/National Weather Service*
1901 South State Route 134, Wilmington, OH 45177-9708
email: daniel.hawblitzel@noaa.gov

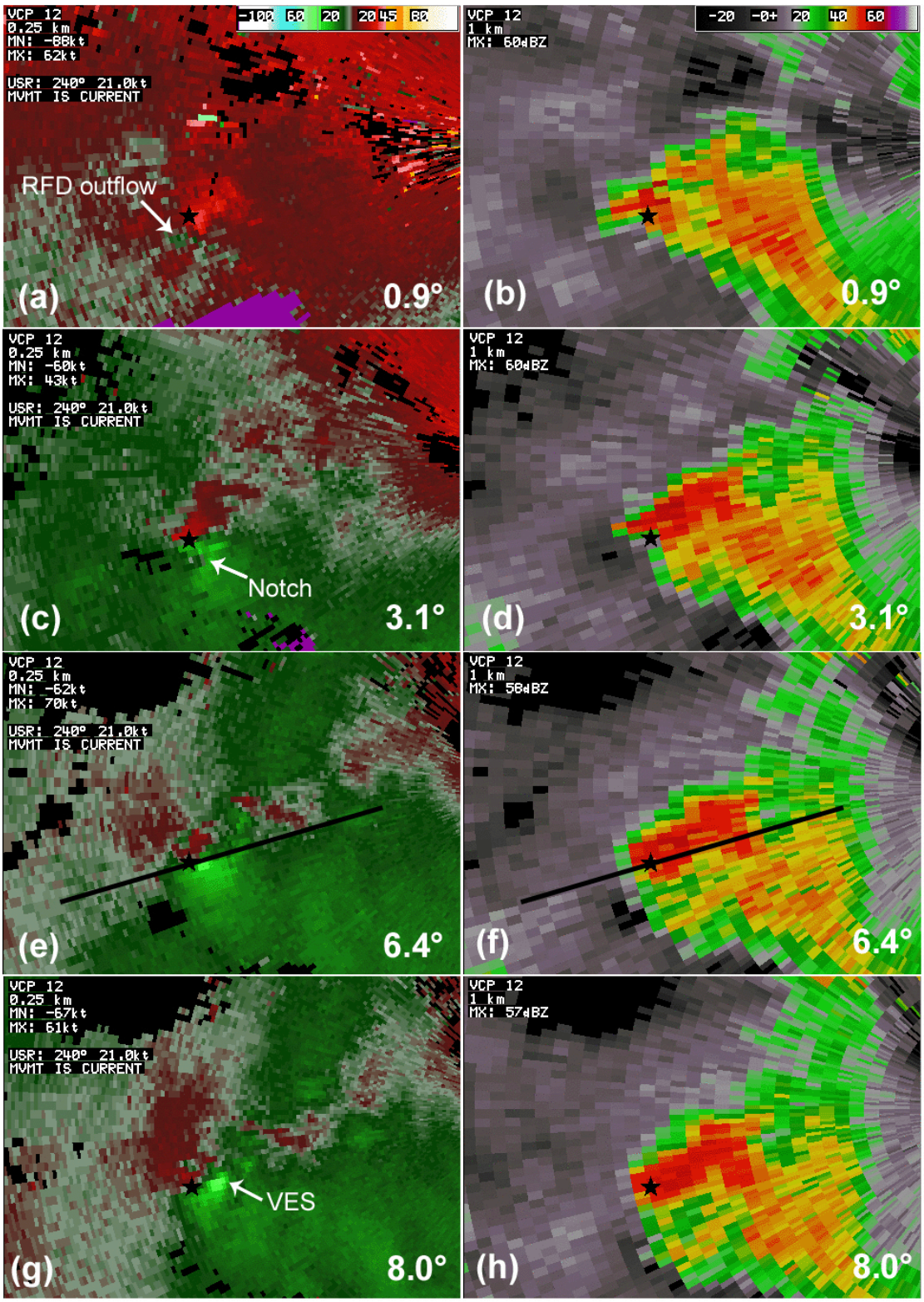

Figure 1. KILN WSR-88D data at 0006 UTC on 12 July 2006 at four different radar tilts, showing storm-relative velocity in (a), (c), (e) and (g), and base reflectivity in (b), (d), (f) and (h). The 0.9° tilt shows the storm around 480 m AGL, the 3.1° tilt around 1.4 km AGL, the 6.4° tilt around 2.7 km AGL and the 8.0° tilt around 3.2 km AGL. The black star denotes the approximate mesocyclone center for reference. The black line denotes the location of the cross section in Fig. 2. The KILN radar is located to the right of the image.

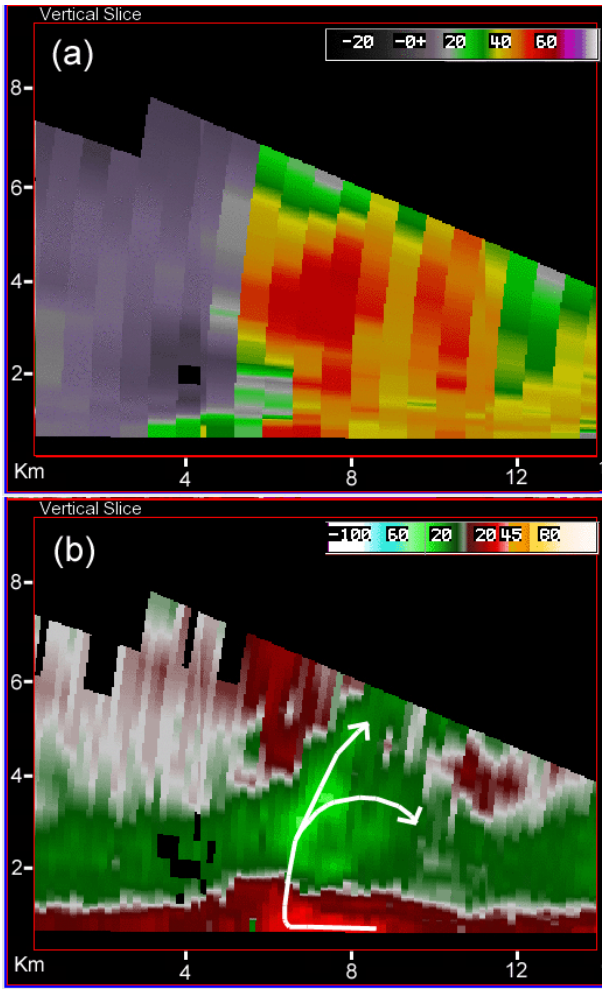

Figure 2. Cross section of KILN WSR-88D data at 0006 UTC on 12 July along the black line in Fig. 1. (a) shows reflectivity and (b) storm-relative velocity. The cross section is taken down-radial, with the radar located to the right of the image.

with storm inflow and convergence near the ground, and storm outflow and divergence near the top of the mesocyclone (Fig. 2). This divergent flow atop the mesocyclone is not the same as storm-top divergence, since the precipitation core extends another 2–3 km above this level. It is likely that the low-level inflow and the associated convergence were enhanced by an upward-directed pressure gradient force induced by dynamic pressure perturbations within the mesocyclone. Conversely, it is presumable that the opposite would hold true *above* the mesocyclone, where a *downward*-directed pressure gradient force would exist along with a zone of *divergence*. The VES may quite possibly be a reflection of this divergent pattern above the mesocyclone, especially given that it appears when the updraft intensifies, and its divergent end is always directly above the mesocyclone. This midlevel jet may also be an eastward deflection of portions of the updraft as it encounters downward acceleration above the mesocyclone. Note that the VES appears around 2.5-3.5 km AGL, which is near the level of rapid updraft deceleration in the CKL simulation of McCaul and Weisman (1996).

With the appearance of divergence above the mesocyclone also comes the emergence of a distinct velocity notch along the southern flank of the mesocyclone (Fig. 1c). This notch appears below a small area of apparent divergence within the mesocyclone (Fig. 1e) and beneath the divergent end of the VES (Fig. 1g). The velocity notch on the southern end of the mesocyclone at 0014 UTC is even better defined by this point (Fig. 3e) and is still located beneath the divergent end of the VES (Fig. 3g). An apparent RFD outflow signature is evident at about 240 m AGL, depicted as westerly storm-relative velocity to the west of the low-level convergent boundary (Fig. 3a). The RFD outflow is nearly vertically aligned with the velocity notch aloft, which suggests that the velocity notch may be a direct indicator of the RFD aloft. Since the velocity notch (RFD) is consistently located near and underneath divergence on the south side of the mesocyclone and the VES, it is proposed here that positive pressure perturbations caused by this divergence may be driving the RFD downward. It should be noted that this single-doppler analysis can only imply divergence, and other terms such as deformation or impingement of environmental winds at the updraft cannot be easily assessed.

Directly between the notch aloft and the RFD outflow near the ground, two distinct regions of weak sheared cyclonic and anticyclonic vertical vorticity have appeared as a couplet (Fig. 3c). The orientation of the couplet (cyclonic to the north, anticyclonic to the south) would imply downward tilting of horizontal vorticity whose vector points northward. This makes sense given that the presumed RFD was descending through westerly vertical shear on the southern flank of the mesocyclone. At the same time, a very small precipitation core developed near the cyclonic member of the vorticity couplet (Fig. 3d). This core traces upward to the main precipitation core of the storm. This signature appears to be a descending reflectivity core (DRC) as defined by Rasmussen et al. (2006). Given the proximity and similar elongated orientation of the DRC to the center of the sheared cyclonic circulation, it is plausible that the cyclonic member of the vorticity couplet is forcing the DRC via dynamic pressure gradients and downward acceleration, somewhat similar to the occlusion downdraft process. In fact, a very weak precipitation core can also be seen aligned with the anticyclonic vorticity member as well (although weak, this additional DRC is evident throughout several tilts of this volume scan and remains associated with the anticyclonic circulation during the next several volume scans). Note that at this time, the forward-flank of the storm suffered considerable loss of reflectivity data as it encountered local clutter suppression around the zero-isodop. Close analysis of the velocity data of each volume scan showed that the areas of interest (the weak echo region, mesocyclone and DRC) were not greatly affected by this data loss since storm-induced wind flow was non-zero in these areas. Later versions

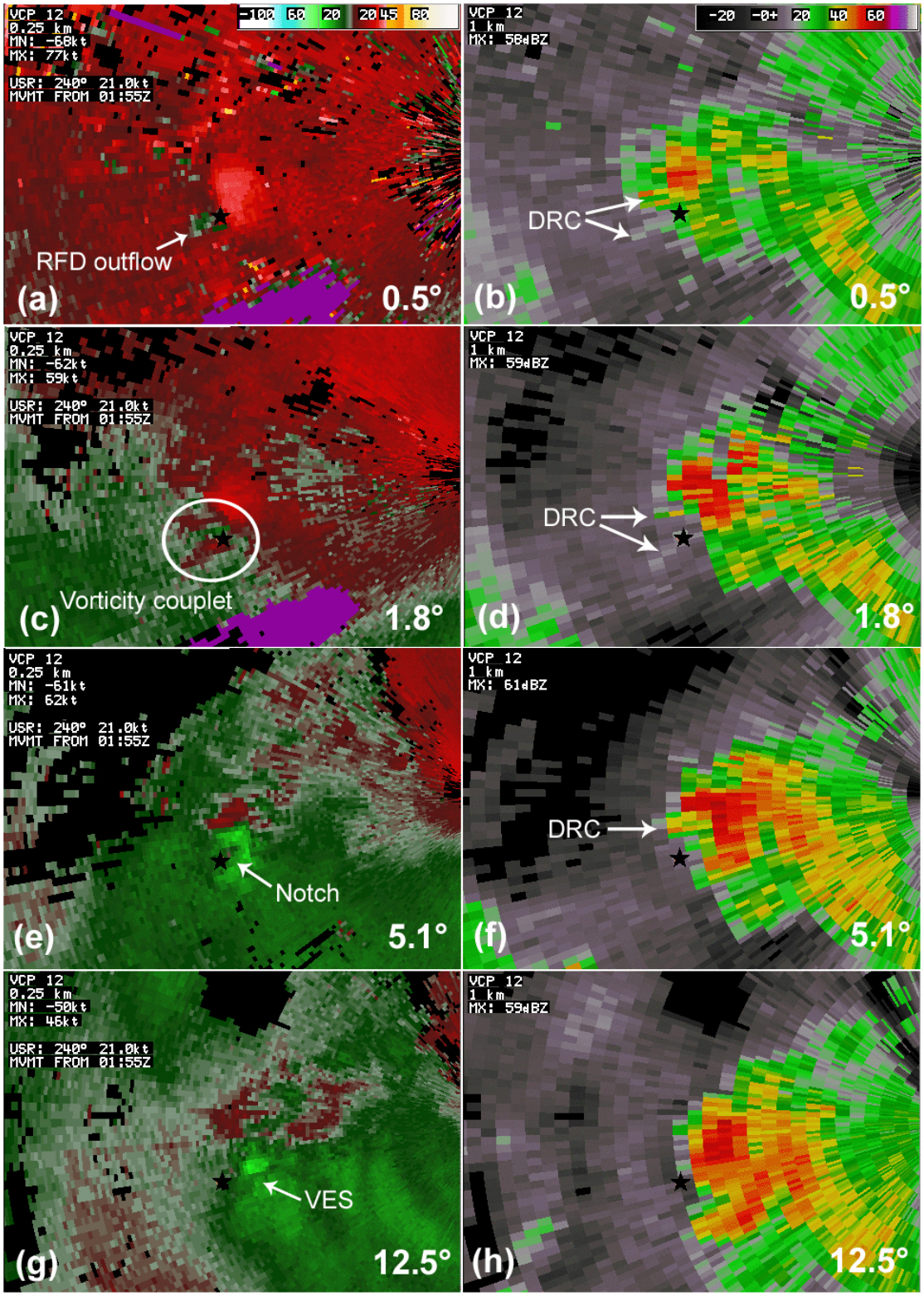

Figure 3. KILN WSR-88D data at 0014 UTC on 12 July 2006 at four different radar tilts, showing storm-relative velocity in (a), (c), (e) and (g), and reflectivity in (b), (d), (f) and (h). The 0.5° tilt shows the storm around 240 m AGL, the 1.8° tilt around 700 m AGL, the 5.1° tilt around 1.8 km AGL and the 12.5° tilt around 4.4 km AGL. The black star denotes the approximate location of the low-level RFD outflow signature for reference. The KILN radar is located to the right of the image.

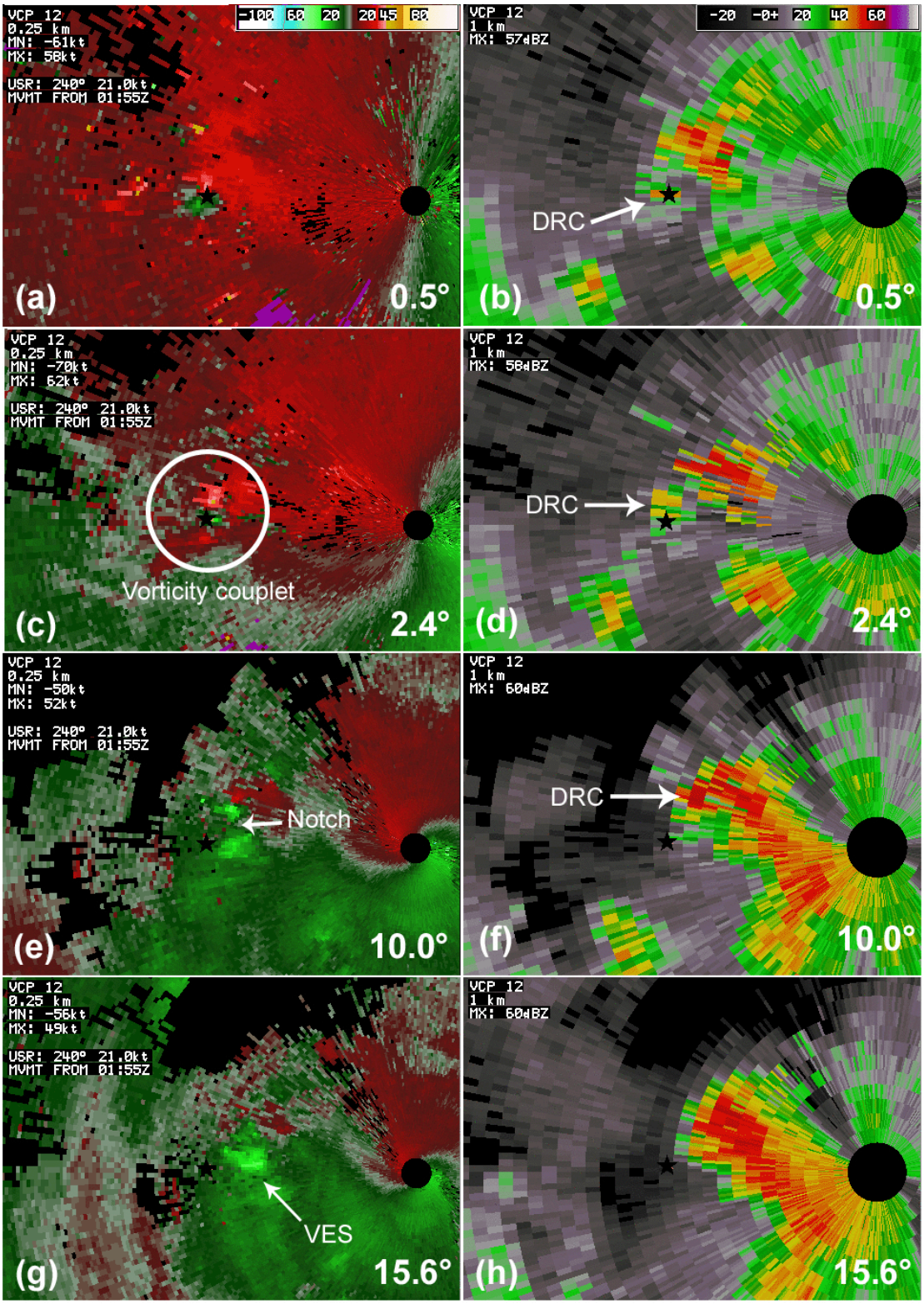

Figure 4. KILN WSR-88D data at 0027 UTC on 12 July 2006 at four different radar tilts, showing storm-relative velocity in (a), (c), (e) and (g), and reflectivity in (b), (d), (f) and (h). The 0.5° tilt shows the storm around 150 m AGL, the 2.4° tilt around 640 m AGL, the 10.0° tilt around 2.5 km AGL and the 15.6° tilt around 3.8 km AGL. The black star denotes the approximate center of the near-ground circulation for reference. The KILN radar is located on the right hand side of the image.

of this study will attempt to restore this data.

Thirteen minutes later, at 0027 UTC (Fig. 4), the vorticity couplet is even better defined (Fig. 4c), while the DRC has grown in size and intensity (Figs. 4b, d). The velocity notch is still located above the center of the vorticity couplet (Fig. 4e) and below the divergent end of the VES (Fig. 4g). By this time, the cyclonic member of the vorticity couplet has intensified notably inside the DRC, cyclonic vorticity has arrived near the ground (Fig. 4a) and the mesocyclone at 2.5 km AGL has shifted entirely to within the upper portion of the DRC (Fig. 4e). This created a vertically-aligned cyclonic vorticity "tube" within the DRC, extending from the surface to the mesocyclone. The circulation near the ground can be seen occluding with the low level convergence boundary that was beneath the storm updraft. Perhaps not surprisingly, a tornado was reported two minutes later.

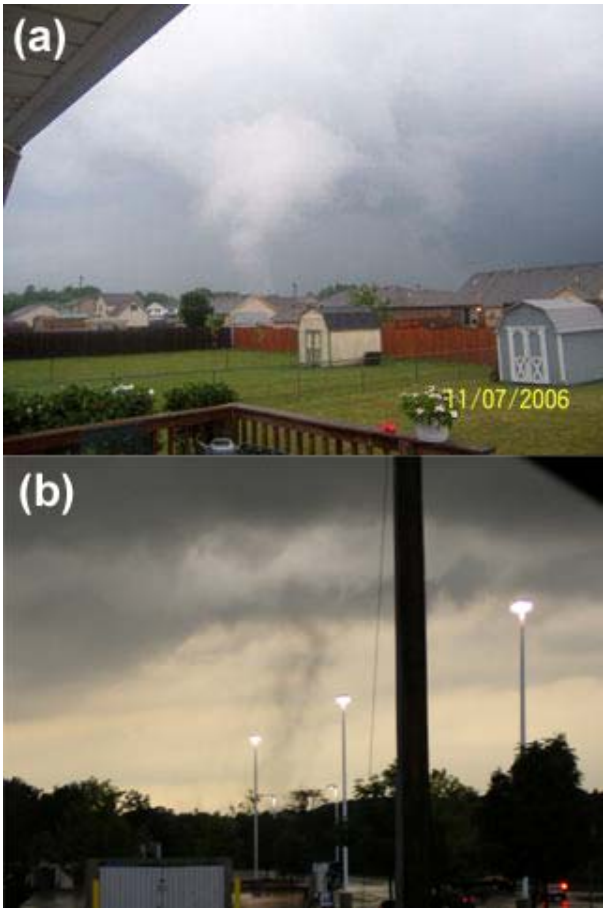

Figure 5. (a) Photograph of a tornado as it struck a residential neighborhood near Carlisle, Ohio on 11 July 2006. Photograph by Rodney Mayo. (b) Photograph of a tornado as it touched down near Mulberry, Ohio on 11 July 2006. Photograph by Craig Floyd. Both photographs used with permission from the photographers.

4. SUMMARY AND DISCUSSION

Given the available radar data, the storm's evolution from mesocyclone formation to tornado-genesis is summarized in the following preliminary proposal:

1) Mesocyclone develops.
2) Dynamic pressure gradient within the mesocyclone enhances upward acceleration and horizontal convergence beneath the cloud base, and results in downward acceleration and horizontal divergence above the mesocyclone.
3) Divergence atop and to the south of the mesocyclone creates a positive pressure perturbation which forces the RFD downward, through the southern flank of the mesocyclone, to the ground.
4) The RFD passes through westerly vertical shear within the southern flank of mesocyclone, and tilts horizontal vorticity so that a vertical vorticity couplet appears beneath the mesocyclone.
5) Negative dynamic pressure perturbations within both members of the vorticity couplet force descent from above. Descent brings precipitation down through the western flank of the mesocyclone, into the cyclonic member of the vorticity couplet. This is the initiation of the DRC.
6) The DRC passes through vertical vorticity within the mesocyclone. This causes stretching and downward transport of cyclonic vertical vorticity within the core of the DRC.
7) As the low-level vorticity increases, the DRC grows and intensifies, possibly through a process similar to an occlusion downdraft. The mesocyclone circulation shifts toward the upper portions of the DRC (possibly due to the dynamic pipe effect) so that low- and mid-level vorticity increase and are aligned as one solid vorticity tube centered directly within the DRC.
8) Vertical cyclonic vorticity arriving near the ground inside the DRC occludes with the convergent inflow boundary beneath the updraft.
9) Tornadogenesis.

These mechanisms all imply baratropic processes. Since almost no thermodynamic data was available from this storm, baroclinic contributions to vorticity, or buoyant contributions to descent, cannot be easily assessed. However, it should be noted that when the forward-flank precipitation core of the storm passed over an observing station in Wilmington at 0030 UTC 12 July, the dewpoint temperature rose one degree Celsius while the surface temperature did not change at all (the ambient temperature/dewpoint spread was only two degrees Celsius to begin with). This may indicate that baroclinicity associated with the storm's cold pool was minimal. The sounding from that evening (shown in Fig. 3 in Hawblitzel 2008) also indicates little potential for evaporative cooling anywhere in the atmosphere, though buoyancy gradients and baroclinicity associated with the melting of hydrometeors and the updraft itself certainly existed.

There are many possible means by which downward acceleration can be forced, both by dynamic

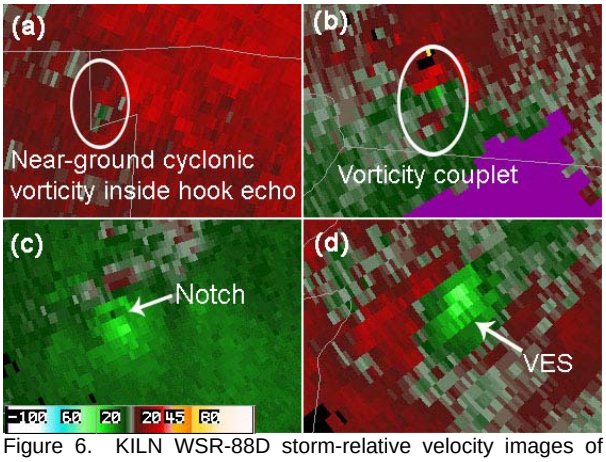

Figure 6. KILN WSR-88D storm-relative velocity images of three different storms on 11 July 2006. (a) the 0.5° SRV of a storm at 2320 UTC as a tornado touched down near Carlisle, Ohio. The cyclonic circulation was contained entirely within the storm's hook echo (not shown). Image shows storm data near 600 m AGL. (b) the 0.5° tilt at 2345 UTC shortly before a storm produced a tornado near Maineville, Ohio. Storm data is around 700 m AGL. (c) the 4.1° tilt of the same storm as the tornado touched down near Maineville. Data is shown at 2349 UTC and shows the storm near 2.2 km AGL. (d) the 6.4° scan of a storm at 0027 UTC 12 July about 30 minutes before a tornado touched down near Goshen, Ohio. Storm data is displayed near 4.6 km AGL.

and buoyant forcing. While this single-doppler analysis cannot thoroughly assess RFD forcing or total values of divergence/deformation from this storm, enough data is available to support the proposal presented here, that divergent flow above the mesocyclone may have forced the RFD through dynamic pressure perturbations. It is noted that storm-relative flow at the level of the velocity notch was relatively weak (generally less than 15 kt), and the notch developed on the southern side of the mesocyclone while storm-relative winds were from the west. Therefore it is conceivable that the RFD was not forced by stagnation of storm-relative winds at the updraft in this case. Also, photographs of two tornadoes from nearby storms do not show a well-defined funnel cloud or wall cloud attached to storm bases, which may suggest these tornadoes developed near the ground and "spun up" instead of descending from the mesocyclone as a funnel cloud (Fig. 5). This would support the idea that tornadogenesis resulted from convergence acting on near-ground vertical vorticity.

This study presents rare high-resolution radar data of a minisupercell. Three of the more significant features of this storm appear to be the low-level vorticity couplet, the velocity notch and the VES. These features were also evident in many other storms that evening despite being further from the radar (including the storm of interest at earlier stages in its lifecycle). Some of these signatures are shown in Fig. 6. To the author's knowledge, little documentation of such features exists, with the exception of the VES, which was introduced just recently in a tropical study involving environments similar to this one. It is unclear if the sheared vorticity couplet in this case is related to the counterrotating shear signatures which have been documented to straddle hook echoes in many cases (see Markowski 2002, for example). In this case, the couplet is oriented differently with respect to the DRC/hook echo (parallel to it rather than perpendicular). It is likely, however, that the couplet is related to the vortices noted to be associated with DRCs in Rasmussen et al. (2006).

While storm dynamics within minisupercells may vary greatly from their Great Plains counterparts, they share many of the same features, so results from this study may be relevant to other storm environments as well. At the very least, the data presented here suggest that future research related to RFD forcing mechanisms may want to focus on pressure perturbations aloft. It may also be beneficial to expand high resolution dual doppler-radar studies to minisupercells, especially in environments similar to this one. Since updrafts in these cases are driven more by dynamic forcing than buoyancy, dual-doppler analyses may come up with valuable insight into supercell dynamics, possibly even extractable to the entire supercell spectrum.

5. ACKNOWLEDGEMENTS

The author would like to express his appreciation to local management at WFO Wilmington, OH (ILN) for their support for this research and paper. A special thanks is owed to John DiStefano, SOO at ILN, for his assistance and allowing me the time to complete this study. The author also wishes to thank Stephen Hrebenach, senior forecaster at ILN, for his assistance and comments, and Dave Radell of Eastern Region Scientific Services Division for his thorough review of this manuscript.

6. REFERENCES

Hawblitzel, D. P., 2008: The southwest Ohio minisupercell tornado outbreak of 11 July 2006. Part I: Mesoscale and radar analysis. Preprints, *24th Conf. on Severe Local Storms*, Savannah, GA, Amer. Meteor. Soc.

Klemp J. B., and R. Rotunno, 1983: A study of the tornadic region within a supercell thunderstorm. *J. Atmos. Sci.,* **40,** 359–377.

Markowski P. A., 2002: Hook echoes and rear-flank downdrafts: A review. *Mon. Wea. Rev.,* **130,** 852–876.

McCaul E. W. Jr., and M. L. Weisman, 1996: Simulations of shallow supercell storms in landfalling hurricane environments. *Mon. Wea. Rev.,* **124,** 408–429.

Rasmussen E. N., J. M. Straka, M. S. Gilmore, and R. Davies-Jones, 2006: A preliminary survey of rear-flank descending reflectivity cores in supercell storms. *Wea. Forecasting,* **21,** 923–928.

Schneider, D., and S. Sharp, 2007: Radar signatures of tropical cyclone tornadoes in central North Carolina. *Wea. Forecasting,* **22,** 278–286.